

Accelerating the Heat Diffusion: Fast Thermal Relaxation of a Microcantilever

Basile Pottier, Ludovic Bellon, Carlos Plata, Emmanuel Trizac, David Guéry-Odelin

▶ **To cite this version:**

Basile Pottier, Ludovic Bellon, Carlos Plata, Emmanuel Trizac, David Guéry-Odelin. Accelerating the Heat Diffusion: Fast Thermal Relaxation of a Microcantilever. Physical Review Applied, 2023, 19 (3), pp.034072. 10.1103/PhysRevApplied.19.034072 . hal-04041907

HAL Id: hal-04041907
https://hal.science/hal-04041907

Submitted on 22 Mar 2023

HAL is a multi-disciplinary open access archive for the deposit and dissemination of scientific research documents, whether they are published or not. The documents may come from teaching and research institutions in France or abroad, or from public or private research centers.

L'archive ouverte pluridisciplinaire **HAL**, est destinée au dépôt et à la diffusion de documents scientifiques de niveau recherche, publiés ou non, émanant des établissements d'enseignement et de recherche français ou étrangers, des laboratoires publics ou privés.

Accelerating the heat diffusion: Fast thermal relaxation of a microcantilever

Basile Pottier and Ludovic Bellon*
Univ Lyon, ENS de Lyon, CNRS, Laboratoire de Physique, F-69342 Lyon, France

Carlos A. Plata
Fisica Teórica, Universidad de Sevilla, Apartado de Correos 1065, E-41080 Sevilla, Spain

Emmanuel Trizac
Université Paris-Saclay, CNRS, LPTMS, F-91405 Orsay, France

David Guéry-Odelin
Université de Toulouse, CNRS, IRSAMC, Laboratoire de Collisions Agrégats Réactivité, F-31062 Toulouse, France
(Dated: March 22, 2023)

In most systems, thermal diffusion is intrinsically slow with respect to mechanical relaxation. We devise here a generic approach to accelerate the relaxation of the temperature field of a 1D object, in order to beat the mechanical time scales. This approach is applied to a micro-meter sized silicon cantilever, locally heated by a laser beam. A tailored driving protocol for the laser power is derived to quickly reach the thermal stationary state. The model is implemented experimentally yielding a significant acceleration of the thermal relaxation, up to a factor 30. An excellent agreement with the theoretical predictions is reported. This strategy allows a thermal steady state to be reached significantly faster than the natural mechanical relaxation.

I. INTRODUCTION

In condensed matter, the temperature fields evolve in general on much longer time scales than their mechanical counterparts (such as stress or strain). Indeed, combining the highest thermal diffusivity in solids [1] ($D \sim 10^{-4}\,\mathrm{m}^2/\mathrm{s}$) and the order of magnitude of the speed of sound [1] ($c \sim [10^3 - 10^4]\,\mathrm{m/s}$), one defines a typical length scale $l_{th} = D/c \sim [10 - 100]\,\mathrm{nm}$ beyond which temperature is a slow phenomenon. Most systems imply larger length scales, thus a slow temperature evolution. In some devices or experiments, or for proof-of-concept demonstrations, it can however be desirable to accelerate the heat diffusion so as to impose a temperature variation on time scales equivalent, or shorter, than those of the mechanical response of the system.

One example is atomic force microscopy (AFM) [2], where a sharp tip attached to a cantilever scans a sample to map its topography and potentially more local properties of its surface. Most commonly, the measure of the interaction force through the deflection of the cantilever is performed with a laser beam [3], hence the photothermal response and thermal stability of AFM-sensors have been extensively studied almost since the origin of AFM [4, 5]. Photothermal excitation has been used in vacuum, air, or fluid, aiming at driving the cantilever efficiently while avoiding overheating of the system [6–11]. Let us compare the relaxation time $\tau = L^2/D$ of the temperature field along the cantilever length L, to the period of oscillation of the first resonance $T_0 \simeq 6.4L^2/(cH)$ [12], with H the thickness of the cantilever: $T_0/\tau \simeq 6.4\, l_{th}/H = 65\,\mathrm{nm}/H$, where the numerical application has been done for silicon [13]. With H typically in the few μm range, thermal diffusion is thus much slower than the oscillation period of the system, limiting the efficiency of photothermal excitation, or the speed of operation of scanning thermal microscopy [14–16].

Another example where fast temperature variations could be desirable is in stochastic thermodynamics experiments on micro-mechanical systems [17, 18] (optically trapped particles, micro-cantilevers, MEMS - micro-electromechanical systems). When constructing a stochastic Carnot heat engine for instance [19–28], one needs to perform adiabatic heating or cooling, that is to say change the system temperature much faster than the time scale τ_r corresponding to the heat exchanges with the thermostat. τ_r is equivalent to the mechanical relaxation time, which writes for a cantilever $\tau_r = QT_0/\pi$, with Q the quality factor of the resonance [17, 29–34]. The situation is thus somewhat more favorable than previously for underdamped systems, but requires quality factors larger than a few hundred to start matching the natural thermal diffusion and mechanical relaxation timescales: $\tau_r/\tau \simeq Q \times 20\,\mathrm{nm}/H$. Here again, an acceleration of the temperature dynamics would be welcome to perform efficient adiabatic transformations.

The motivation of this work is to speed up the natural thermal relaxation, and we focus in this article on the case of a cantilever, in relation to the previously mentioned examples. Engineered accelerated dynamics and shortcuts are protocols of the 'Shortcut to Adiabaticity' type [35]. This class of ideas emerged in the quantum realm [36, 37]. Yet, a number of techniques belonging to this family of accelerating methods has been successfully exported to classical and stochastic dynamics [28, 38–41]. Some of these shortcuts are of inverse engineering type,

* ludovic.bellon@ens-lyon.fr

requiring a careful monitoring of the time dependence of some control parameters, to impose a prescribed evolution of interest [39]. Such accelerating protocols have also been used fruitfully in systems such as cranes [42] and capacitors [43].

In the following, we address the question of the temperature field control, so far untouched. The goal is to drive the thermal relaxation of a micro-cantilever in a time much smaller than its natural relaxation time. First, we model the thermal relaxation and derive theoretically the accelerating protocols allowing the reduction of the relaxation time of the cantilever to reach thermal steady state. Second, the aforementioned protocols are experimentally implemented in a silicon cantilever. The efficacy of the driving is patent when comparing to a direct relaxation process. Moreover, experimental results are in full agreement with the predictions. Finally, we summarize the conclusions of our study and mention future perspectives.

II. THEORY

Our objective is to accelerate the relaxation towards a non-equilibrium steady state of a cantilever with a tunable punctual and well-localized heat source. To this end, we first identify the different eigenmodes (and corresponding timescales) of the heat equation that governs the dynamics of the system. We subsequently design the rate at which the deposit of heat should be carried out so as to cancel the contribution of the low frequency eigenmodes that slow down the relaxation. This original trick enables one to benefit from a fast relaxation with the cancelation of just a few modes.

A. Temperature rise of a cantilever irradiated by a laser beam

We gather here the main ingredients useful for a quantitative description of the temperature field of a cantilever irradiated by a laser beam. As the cantilever is placed in vacuum, no heat transfer can occur by convection with its surroundings. Neglecting thermal radiation, the only possible heat transfer mechanism is thus thermal conduction through the cantilever. Considering a cantilever having a length L much larger than its transverse dimensions, the temperature θ may be assumed homogeneous across the cross section. Therefore, θ depends only on the longitudinal coordinate $x \in [0, L]$ and time t, its dynamics being described by the one-dimensional heat diffusion equation

$$\rho c_p \frac{\partial \theta(x,t)}{\partial t} = \lambda \frac{\partial^2 \theta(x,t)}{\partial x^2} + q(x,t), \tag{1}$$

where ρ is the density, c_p is the heat capacity, λ is the thermal conductivity (all of them assumed constant), and q is the heat source/sink density. In vacuum, all cantilever surfaces are assumed to be thermally insulated, except at the location x_0 irradiated by the focused laser. We model the heating effect of the focused beam by the source term

$$q(x,t) = \frac{aP(t)}{S}\delta(x - x_0), \tag{2}$$

where a is the fraction of light absorbed by the cantilever, $P(t)$ is the incident power of the laser beam which can be manipulated at wish, S is the cantilever cross section area, and δ Dirac's distribution. Furthermore, we assume the following boundary conditions

$$\theta(0,t) = 0, \tag{3a}$$

$$\frac{\partial \theta}{\partial x}(L,t) = 0. \tag{3b}$$

These conditions reflect respectively that the cantilever is in contact with the macroscopic chip acting as a thermostat at its clamp $x = 0$ (3a), and is isolated on its free end $x = L$ (3b). Note that, for the sake of simplicity, θ is not the absolute temperature, as we define the origin by the temperature of the chip.

B. Stationary profile θ_s

The stationary temperature profile $\theta_s(x)$ associated to a given power of the laser P_f is obtained solving Eq. (1) where $\partial\theta/\partial t = 0$, with the boundary conditions Eq. (3). We get

$$\frac{\theta_s(x)}{\theta_s^m} = \begin{cases} x/x_0, & 0 < x < x_0, \\ 1, & x_0 < x < L, \end{cases} \tag{4}$$

where $\theta_s^m = aP_f x_0/(S\lambda)$ corresponds to the maximum temperature elevation. Between the chip and the laser spot ($x = x_0$), the stationary temperature increases linearly with the position x, while beyond the laser spot, it remains constant and equals θ_s^m.

From now on, we focus the analysis on the relaxation between two stationary states when driving the power $P(t)$ from a constant initial value $P(t < 0) = P_0$ to its constant final value $P(t > t_f) = P_f$. Note that even if $P(t)$ is constant after the final time t_f, the temperature profile continues to evolve towards its final asymptotic stationary shape. Since the heat diffusion equation (Eq. 1) is linear, we make the simplifying assumption that $P_0 = 0$: without loss of generality, $P(t)$ or P_f represent the laser power excess with respect to P_0, and $\theta(x,t)$ or $\theta_s(x)$ stand for the temperature excess with respect to the initial stationary temperature profile.

C. Transient solution through expansion

The general solution of Eq. (1) can be expressed carrying out an expansion in eigenfunctions $\psi_n(x)$ [44, 45],

each satisfying the associated homogeneous problem $\partial_{\tilde{x}}^2\psi_n(\tilde{x}) = -k_n^2\psi_n(\tilde{x})$ with $\psi_n(0) = 0$ and $\psi_n'(L) = 0$. Solving the homogeneous problem leads to

$$\psi_n(\tilde{x}) = \sqrt{2}\sin(k_n\tilde{x}), \quad \tilde{x} = x/L \tag{5}$$

with the eigenvalues $k_n = (n-1/2)\pi$, $n \in \mathbb{N}^*$. The temperature profile can be expressed as

$$\theta(x,t) = \theta_s(x) + \theta_s^m \sum_{n=1}^{\infty} C_n(\tilde{t})\psi_n(\tilde{x}), \tag{6}$$

where the components $C_n(\tilde{t})$ depend solely on $\tilde{t} = t/\tau$, with $\tau = \rho c_p L^2/\lambda$, the characteristic diffusion time of the problem. These components are obtained projecting Eq. (1) on the eigenmodes basis $\psi_n(x)$; they read as

$$C_n(\tilde{t}) = \frac{\psi_n(\tilde{x}_0)}{\tilde{x}_0}\left[\int_0^{\tilde{t}} \big(F(s\tau)-1\big)e^{k_n^2 s}ds - \frac{1}{k_n^2}\right] e^{-k_n^2\tilde{t}}, \tag{7}$$

with $\tilde{x}_0 = x_0/L$, and F the driving function defined as

$$F(t) = \frac{P(t)}{P_f}. \tag{8}$$

The temperature solution Eq. (6) is completely general for arbitrary $F(t)$, even though here $F(t<0) = 0$ and $F(t>t_f) = 1$ by construction. For $t > t_f$, the bracket term in Eq. (7) is constant, so each component in the expansion decays exponentially with its own decaying rate. Specifically, the n-th component has a rate equal to k_n^2, which increases with the mode number n as $(2n-1)^2$: the second mode decays $k_2^2/k_1^2 = 9$ times faster than the fundamental mode, the third mode decays $k_3^2/k_1^2 = 25$ times faster than the fundamental one, etc. The higher the mode n, the less time it takes for that component of the temperature to relax.

D. Accelerating the dynamics

We explain hereafter how the driving function can be designed to remove the contribution of the slow relaxation modes, thereby speeding up the relaxation dynamics in a given arbitrary small (chosen) time lapse t_f. Our strategy is somewhat similar to that of Ref. 46 on a different thermal acceleration problem. For this purpose, we use an ansatz for $F(t)$ that involves as many parameters as modes to be canceled. Let us assume that we want to cancel the N first modes. We can take the following convenient polynomial ansatz

$$F(t) = \sum_{m=1}^{N} \gamma_m \left(t/t_f\right)^{m-1}, \quad 0 < t < t_f. \tag{9}$$

Canceling the N first modes corresponds to impose $C_n(\tilde{t}_f) = 0$ for $n = 1$ to N, where $\tilde{t}_f = t_f/\tau$. This

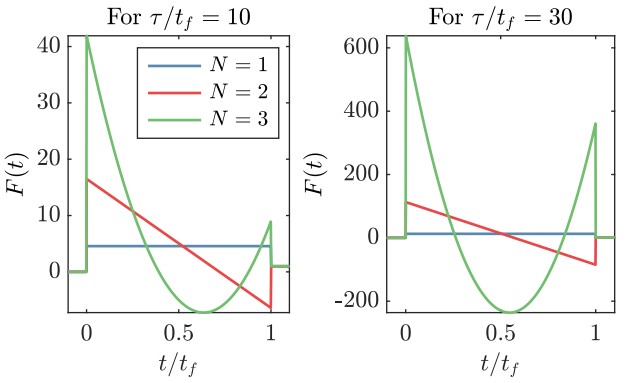


FIG. 1. Driving function $F(t)$ to apply in order to cancel successively the first thermal modes for an acceleration (towards the stationary profile) such that $t_f = \tau/10$ (left) and $t_f = \tau/30$ (right). The coefficients γ_n defining $F(t)$ are found solving Eq. (10); they are listed in table I of Appendix A.

implies for $n \in [1, N]$

$$\sum_{m=1}^{N} \gamma_m \int_0^{\tilde{t}_f} \left(\frac{s}{\tilde{t}_f}\right)^{m-1} e^{k_n^2 s}ds = \frac{e^{k_n^2\tilde{t}_f}}{k_n^2} \tag{10}$$

which is a system of N linear equations for N unknown variables γ_n, analytically solvable. When t_f is reached, we change the laser power abruptly to P_f (i.e. $F(t>t_f) = 1$) and the relaxation will occur only through the modes higher than the N-th one (since we already force the cancelation of the first N modes). Examining Eq. (10), the coefficients γ_n depend only on the normalized protocol duration $\tilde{t}_f$ and the number of canceled modes N; the protocol to apply thus does not depend on the laser beam position $\tilde{x}_0$. For the sake of concreteness, we illustrate our protocols with $\tilde{x}_0 = 0.95$ (we exemplify the independence of the protocol on $\tilde{x}_0$ by working out the solution for $\tilde{x}_0 = 0.5$ in Appendix B). If one wants only to cancel the relaxation of the fundamental mode ($N = 1$), the function $F(t)$ to apply during the protocol is constant and equals $1/(1-e^{-k_1^2\tilde{t}_f})$; for $\tilde{t}_f = 0.1$, we have $F(t) = 4.57$. In Fig. 1, we show the functions $F(t)$ that allow the cancelation of up to the third mode for a protocol duration $\tilde{t}_f = 1/10$ and $\tilde{t}_f = 1/30$. Further details on the computation and properties of $F(t)$ are given in Appendix A. The needed range of $F(t)$ (thus the laser power) increases with both the number of canceled modes N and the acceleration factor τ/t_f. Note that for $N > 1$, $F(t)$ requires both positive and negative values. In practice, the cantilever can only absorb the power from the laser beam. However, $P(t)$ corresponds to the power excess with respect to the initial value P_0, so that the protocol will be valid as long as P_0 is larger than $-\min[P(t)]$. A priori, this constraint implies a limitation for our protocols. However, we prove below that our method succeeds in accelerating thermal relaxation substantially in a wide variety of experimentally realizable situations.

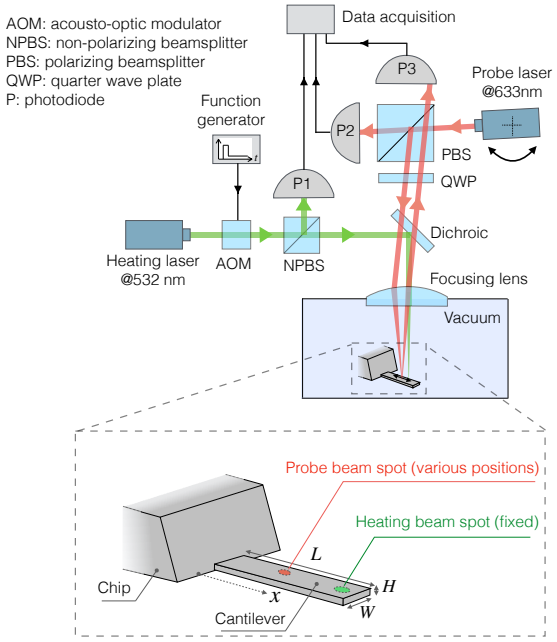


FIG. 2. Sketch of the experimental setup. The heating laser beam (at 532 nm) is fixed and focused at the extremity of a cantilever placed in vacuum. The power of the heating beam is modulated with an acousto-optic modulator. The probe laser beam (at 633 nm) is used to measure the local temperature change by analyzing the cantilever reflectivity variations. By tilting the probe laser, the probe beam spot scans the cantilever length allowing the measurement of the temperature variation at different positions x.

III. EXPERIMENTAL RESULTS

A. Experimental setup

For the experiments presented below, a silicon cantilever placed in vacuum is heated with a laser and the evolution of its temperature at various positions x along its length L is measured.

At a thickness of a few micrometers, silicon is semi-transparent for visible light, the light experiences multiple reflections within the thickness of the cantilever, which acts as a lossy Fabry-Perot [47]. As a result, the fraction of light reflected R depends on the thickness and the silicon refractive index, both varying with temperature θ. By measuring the local change in reflectivity, one can thus infer the local temperature variation with respect to the reference temperature field. For small variations, we have $\Delta R(x)/R(x) = \beta\theta(x)$, where the sensitivity β depends on the local properties (refractive index and thickness). The calibration procedure for β is detailed in Appendix C.

The experimental setup comprises two laser beams (Fig. 2): (i) a heating laser beam (at 532 nm) of variable power $P(t)$ focused at a fixed position close to the cantilever free end ($x_0 = 0.95L$) that serves to heat the cantilever, and (ii) a probe laser beam (at 633 nm) of constant power (350 μW) that allows us to measure the local temperature rise taking benefit of the thermo-optical effect described above. The radius of the heating and probe beam at the cantilever surface are respectively 14 μm and 7 μm. The power of the heating beam is modulated with an acousto-optic modulator, with a rise time of 100 ns. Three photodiodes $P1$, $P2$, and $P3$ measure the incident heating beam power $P(t)$ and the reflectivity R of the probe beam respectively, as shown in Fig. 2. By tilting the probe laser, one scans the cantilever length facilitating temperature measurements at various locations x.

During the experiment, the cantilever is placed in vacuum at 2×10^{-2} mBar. At this pressure level, the contribution of convective heat transfer is negligible compared to thermal conduction [8]. All the measurements are performed using a single raw silicon cantilever OCTO-1000D from Micromotive, with the following size: length $L = 1$ mm, width $W = 90\,\mu$m and thickness $H = 5\,\mu$m.

To record the spatial dependence of the temperature profile, we choose 20 evenly spaced positions x of the probe beam along the cantilever. At each position, we measure the time evolution of the temperature $\theta(t)$ induced by the applied incident power $P(t)$ of the heating beam. To increase the signal-to-noise ratio, the displayed temperature variations are obtained averaging over 700 heating procedures at each x. The spatial resolution is approximately the size of the laser spot, 7 μm, hence smaller that 1 % of the cantilever length.

B. Relaxation for a step function ($F(t) = 1$)

Before testing the performance of the accelerating protocols worked out in section II, we first present the results obtained imposing a jump in power, $P(t) = P_f$ for $t > 0$. The analysis of the temperature relaxation allows measuring the characteristic diffusion time τ needed to determine the function $F(t)$, to later successfully accelerate the dynamic given a protocol duration t_f. Moreover, this is the simplest reference that can be thought of and it defines the timescale that we would like to beat.

In Fig. 3 and in the movies available as ancillary files [48], we display the cantilever temperature rise measured imposing a sudden increase in the power of $P_f = 5.6\,\mu$W. The heating laser spot is focused close to the free end of the cantilever at $x_0 = 0.95L$. The convergence of the temperature profile towards the expected linear stationary profile given by Eq. (4) confirms that for the temperature variations explored, the silicon conductivity λ can be assumed constant. The maximum temperature elevation is $\theta_s^m = 38$ mK, this value is consistent with the theoretical one $\theta_s^m = aP_f x_0/(WH\lambda)$ with $\lambda = 156\,\mathrm{W\,m^{-1}\,K^{-1}}$ [49] and $a = 0.5$, an absorption coefficient also consistent with the $H = 5\,\mu$m thickness of the cantilever [47].

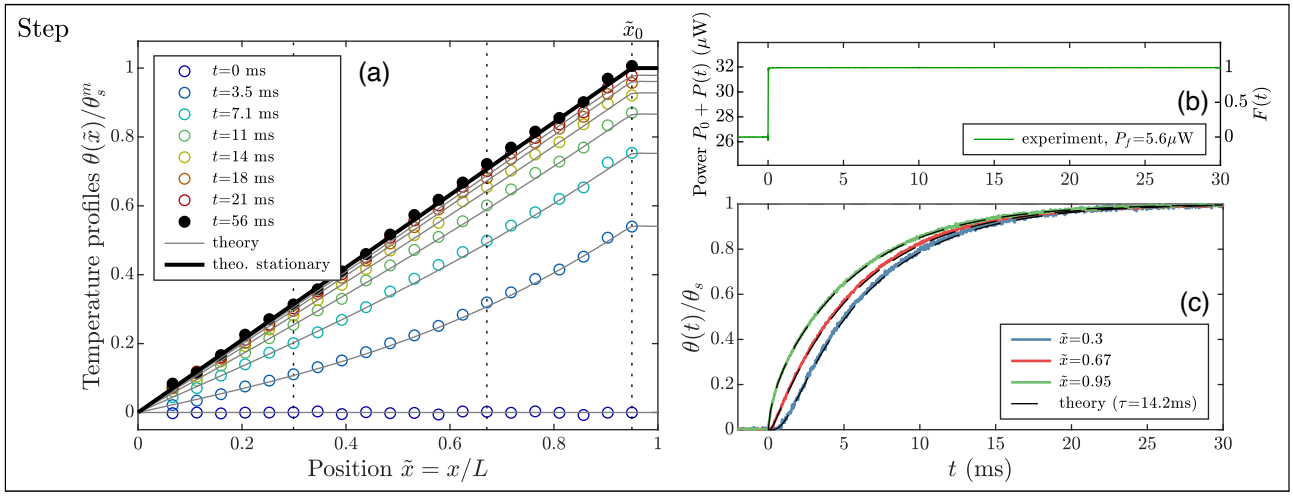


FIG. 3. Transient temperature profiles (a) of a cantilever heated by a laser whose incident power $P(t)$ is the step function (b). The heating laser is located near the cantilever free end ($\tilde{x}_0 = 0.95$). The 5.6 μW increase in power induces a maximum temperature elevation of $\theta_s^m = 38$ mK. As time goes on, the temperature profile converges towards the expected linear stationary profile given by Eq. (4). Graph (c) shows the normalized evolution of temperature at the positions $\tilde{x} = 0.3$, 0.67 and 0.95, corresponding to the vertical dashed lines in panel a). All experimental data are perfectly described by the model of Eq. (6), using the characteristic time $\tau = 14.2$ ms.

In the case of a step function ($F(t) = 1$), the temperature is predicted by Eq. (6) where the components $C_n(\tilde{t})$ are reduced to

$$C_n(\tilde{t}) = -\frac{\psi_n(\tilde{x}_0)}{\tilde{x}_0}\frac{1}{k_n^2}e^{-k_n^2\tilde{t}}. \qquad (11)$$

Using Eq. (11), all experimental data are properly described by theory for a characteristic time τ=14.2 ms. From the thermal diffusivity of bulk silicon given in the literature [49], $D = \lambda/\rho c_p = 86\,\mathrm{mm}^2/\mathrm{s}$, we expect $\tau = L^2/D = 11.6$ ms. The 18% difference could be explained by the reduced diffusivity of silicon due to the phonon confinement effect. Indeed, for a 5 μm thick film, the silicon conductivity is expected to be approximately 15% smaller than the value for bulk silicon [50].

C. Relaxation for an acceleration factor $\tau/t_f = 10$

In Fig. 4, and in the movies available as ancillary files [48], we display the evolution of the measured cantilever temperature when applying the driving function $F(t)$ given by Eq. (9) for a protocol duration $t_f = 1.4$ ms, corresponding to $\tilde{t}_f = 0.1$. We test our protocol varying the number of canceled modes N from 1 up to 4. Note that the imposed functions $F(t)$ correspond to the ones already presented in Fig. 1 (left panel). In order to be able to impose the negative variations in $F(t)$ (for $N > 1$), we choose a reference incident power of $P_0 = 210\,\mu$W. As the number of canceled modes N increases, the temperature at the end of the protocol ($t = t_f$) clearly converges towards the stationary profile $\theta_s(x)$ (Fig. 5). Contrary to the step function (Fig. 3), the temperature takes intermediate values higher than the stationary target $\theta_s(x)$. The maximum transient temperature is obtained for $N = 4$ and corresponds to $\theta = 4.7 \times \theta_s^m$ at $x = 0.95L$. For each protocol, we compare the experiment to theory computing the temperature from Eq. (6) limiting the infinite sum to 60 terms; all experimental data remarkably coincide with theory.

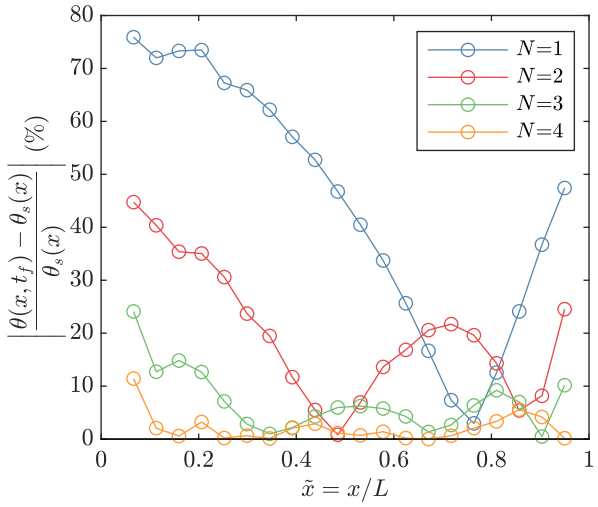


FIG. 5. Relative temperature difference from the targeted stationary profile $\theta_s(\tilde{x})$ at the end of the protocol $t = t_f = 0.1\tau$. As the number of canceled modes N increases, the temperature profile converges towards the stationary profile. For $N = 4$, the relative temperature difference remains below 10% along the cantilever length.

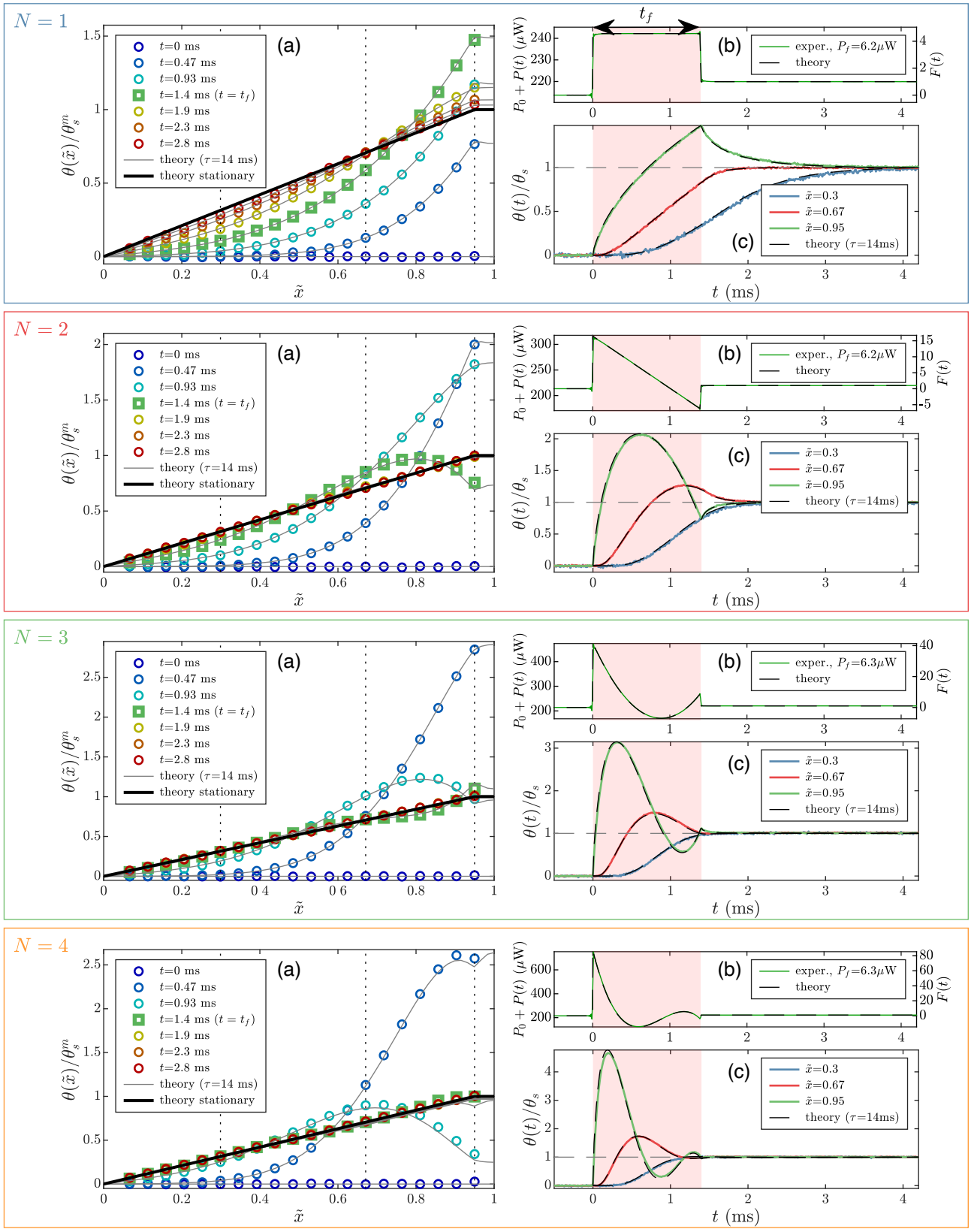


FIG. 4. Transient temperature profiles measured when applying the protocol function $F(t)$ given by Eq. (9) with a protocol duration $t_f = 0.1\tau$ designed to cancel the N first thermal modes. For each tested protocol ($N = 1$ up to $N = 4$) we display (a) the temperature profiles, (b) the imposed power $P(t)$, and (c) the temperature variations with time at the positions $\tilde{x} = 0.3$, 0.67 and 0.95. All experimental data coincide with the expected theoretical temperature variations.

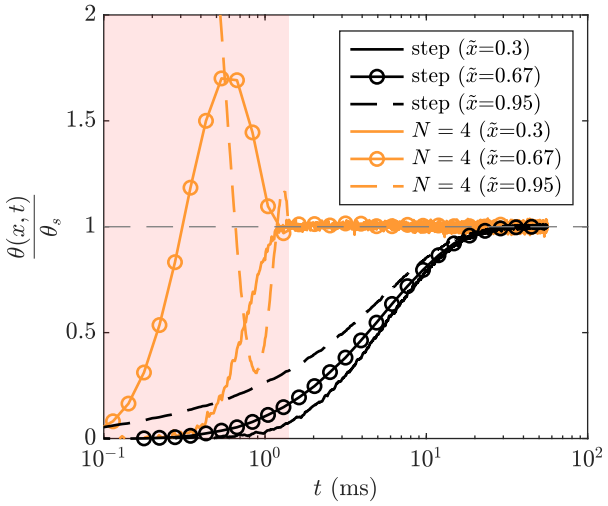


FIG. 6. Comparison of the temperature convergence towards the stationary profile θ_s when heating the cantilever with a step function power (black) or with the accelerating protocol function of Eq. (9) for $N = 4$ (orange). The red shaded area corresponds to the protocol duration, $t_f = 0.1\tau = 1.4\,\text{ms}$.

To highlight the success of our tailored acceleration, we compare in Fig. 6 the difference of convergence towards the stationary profile θ_s between the step function power (displayed in Fig. 3) and the accelerating protocol for $N = 4$ (displayed in the last panel of Fig. 4). Using the step function, the duration needed to converge within 2% (at the positions $\tilde{x} = 0.3, 0.67$ and 0.95) is 25 ms (1.8τ), while in the accelerating protocol this milestone is reached at the end of the program $t_f = 1.4\,\text{ms}$ (0.1τ), beating remarkably the natural relaxation time. Actually, having gotten rid of the first four modes, the fifth and higher orders do remain and are responsible for a slight mismatch with respect to the target profile. They decay at least $9^2 = 81$ times faster than the power step-forcing relaxation, with time scales smaller or equal to $\tau/(4.5\pi)^2 \simeq 0.07\,\text{ms}$, much smaller than t_f itself. Hence, since the characteristic evolution timescale (after t_f) is $k_{N+1}^{-2}\tau$, high values of N are needed for extremely low values of t_f/τ only.

D. Relaxation for an acceleration factor $\tau/t_f = 30$

In Fig. 7(a), we compare the temperature convergence towards the stationary state varying N for a shorter protocol duration of 0.47 ms corresponding to $\tau/t_f = 30$. The driving functions applied, $F(t)$, correspond to the ones displayed in Fig. 1 (right panel). To be able to impose the large variations in $F(t)$, a reduced target power change $P_f = 0.6\,\mu\text{W}$, implying a maximum temperature elevation of $\theta_s^m = 5\,\text{mK}$, is considered. To maintain the signal-to-noise ratio, each curve displayed is now obtained averaging over 3000 measurements. As observed previously for the slower acceleration of $t_f = \tau/10$, the

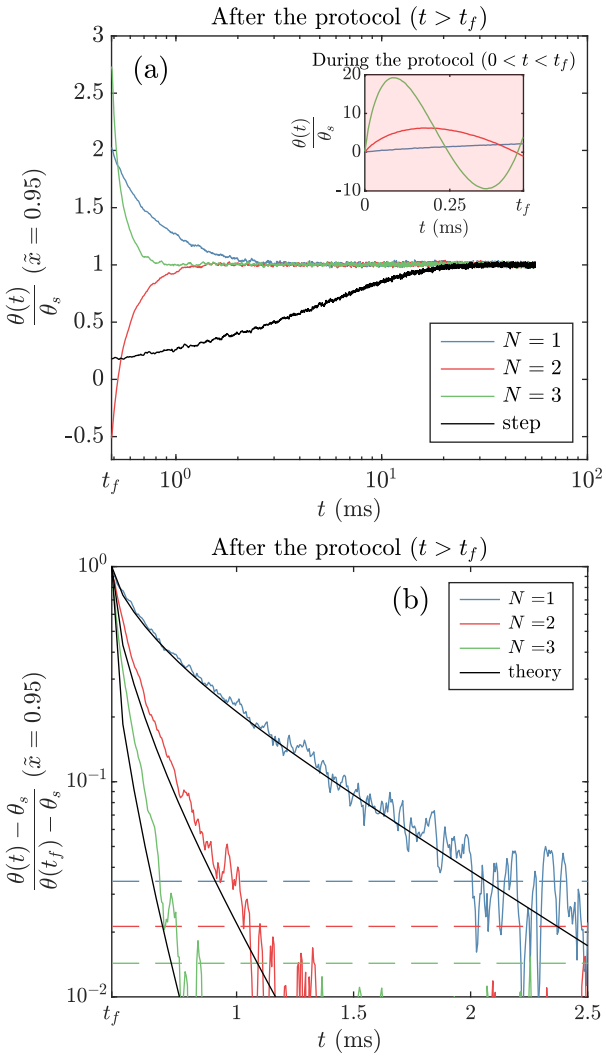


FIG. 7. (a) Temperature relaxation towards the stationary state (measured close to the cantilever free end $\tilde{x} = 0.95$) varying N for a protocol duration $t_f = \tau/30 = 0.47\,\text{ms}$. Inset: temperature variations during the protocol. (b) Comparison of the temperature decay. The horizontal dashed lines correspond to a relative difference $(\theta - \theta_s)/\theta_s$ of 4%.

temperature variations during the protocol duration (see inset) increase with the number of canceled modes N. Note that the transient temperature variations are now much larger and can take negative values.

In that case, the temperature at the end of the protocol is notably different from the stationary value θ_s. The relative difference $(\theta(t_f) - \theta_s)/\theta_s$ (measured at $\tilde{x} = 0.95$) is respectively 100%, -150% and 170% for N increasing from 1 to 3. It may seem counter-intuitive that the difference from the target value obtained at the end of the protocol increases with the number of canceled modes. We recall that our protocol allows converging towards the stationary profile at the end of the protocol only in the limit $N \to \infty$. For a finite value N the use of the protocol guarantees that starting from t_f only the modes

higher than N will relax. Because the rate of relaxation (equal to $k_n^2\tau$) increases with the mode number n, increasing N should allow a faster convergence towards the stationary profile. It cannot be guaranteed that the coefficients of the modes higher than the N-th one take small values at $t = t_f$, but its relaxation is ensured to be exponential, faster and faster for increasing n. Numerical resolution of the heat equation with our protocols are provided in Appendix D, quantifying the limitation caused by these modes surviving after t_f. In Fig. 7(b), we verify that the temperature starting from t_f relaxes faster as N increases, as predicted. For $N = 3$ for example, the relaxation times are at most $\tau/(3.5\pi^2) \simeq 0.12\,\mathrm{ms}$, smaller than t_f itself, and in agreement with the observation (green curve).

IV. DISCUSSION AND CONCLUSIONS

In this work, we tailor in time the power of a localized irradiating laser, in order to speed up the thermal relaxation of a micro-cantilever in a duration much smaller than its natural relaxation time. The protocol duration can be reduced, in principle, as much as desired. In practice however, a smaller duration unavoidably translates into a larger dynamics of the heating/cooling power (minimum and maximum power with respect to final value, faster time control of the imposed drive), and of the transient values of the temperature field. Experimentally, acceleration factors up to a factor 30 are demonstrated.

The theoretical approach relies on canceling the first N eigenmodes of the thermal diffusion equation in a finite time. Of course, the system is getting closer to the exact steady states as more N are considered. Nevertheless, we prove that for an experimentally accessible range of parameters, relatively small values of N may suffice, $N = 4$ providing a *final* state already very close to the stationary one. We emphasize that such a strategy to speed up a given dynamics described by partial differential equations is generic, and can be applied to a wide variety of mesoscopic systems [43]. It complements the methods that have been recently developed in stochastic thermodynamics to speed up a relaxation process [28]. Our approach requires that local equilibrium holds at all times, which allows us to define the temperature field and ensure the validity of Eq. (1). The specific case worked out here also requires that a 1D description of the system is valid, thus that the accelerated dynamics is still slow with respect to the transverse directions of the cantilever. With a width to length ratio of $W/L = 0.09$ in our experiments, the transverse relaxation time is $(W/L)^2\tau = 8.10^{-3}\tau$, smaller than the smallest t_f we probe, but it could be an issue for more ambitious accelerations !

Some driving protocols require a heat sink (negative power), which is technically impossible with laser absorption. From the experimental point of view, this represents a technical problem that is bypassed by choosing a heated initial state. This trick allows the redefinition of the driving function with an offset that gives access to effective negative powers. With our notation, $P_0 + P(t)$ needs to remain positive. Our solution is proven to work in all the considered processes.

Let us point out that our approach is quite different from classic feedback control methods. Those would typically rely on measuring the temperature in one position, say x_0, and adjusting the heating power to reach the setpoint, θ_s^m. A perfect feedback loop would therefore achieve $\theta(x_0, t > 0) = \theta_s^m$, acting as an effective boundary condition (a temperature step at the specific point x_0) for the heat equation (1). The typical time scale to reach the stationary state would then be $x_0^2/(\pi^2 D)$ (see Appendix E), close to one fourth of the power step slowest decay time $4L^2/(\pi^2 D)$: only a 4 times acceleration of the global dynamics would consequently be achieved. Note that reaching the stationary value in one point is very different from reaching the final profile at every position. As a further illustration, we superimpose in the movies available as ancillary files [48] the time evolution of the temperature field in response to a power step, to a temperature step (perfect feedback loop), and to our protocols. The acceleration provided by our strategy is clear, at the expense of noticeable local temperature oscillations and overshoots.

The order of magnitude of the temperature jumps that we experimentally perform is modest: 38 mK for a 10 times acceleration, and 5 mK for a 30 times acceleration. This choice hinges upon a practical consideration: linearity and dynamic range. The thermal conductivity of silicon depends on temperature in a noticeable way (roughly as $\lambda \propto 1/T$ [49]), so that we would like to avoid large temperature excursions to match the linearity hypotheses of the model. Moreover, we need an initial power P_0 to allow negative values for $P(t)$, hence the initial temperature profile is actually not flat. For the set of data presented in Figs. 3 to 6, the maximum temperature due to $P_0 = 210\,\mu$W and the $350\,\mu$W of the red laser probe beam is 4 K, corresponding to a variation of λ below 1.3%. Larger P_0, allowing larger P_f, would imply non uniform values for λ, again deviating from the model. Our goal in this article is to demonstrate the excellent agreement between theory and experiment, so we restrict ourselves to small temperature jumps. We also test larger steps corresponding to $\theta_s^m = 1\,$K, and as illustrated in Fig. 8, the protocols work fine with only tiny adjustments to the parameter τ to compensate for emerging non-linearities. In this case, the maximum temperature due to $P_0 = 400\,\mu$W and the $600\,\mu$W of the red laser probe beam is 50 K, corresponding to a non-uniformity of λ of 16 %.

Larger jumps would require the simple form of the dynamic evolution that facilitates the theoretical derivation of the driving protocol to be reconsidered. The introduction of linear corrections or even non-linearities in λ constitutes a challenging future perspective. One way to partially avoid the need for an extended power range is

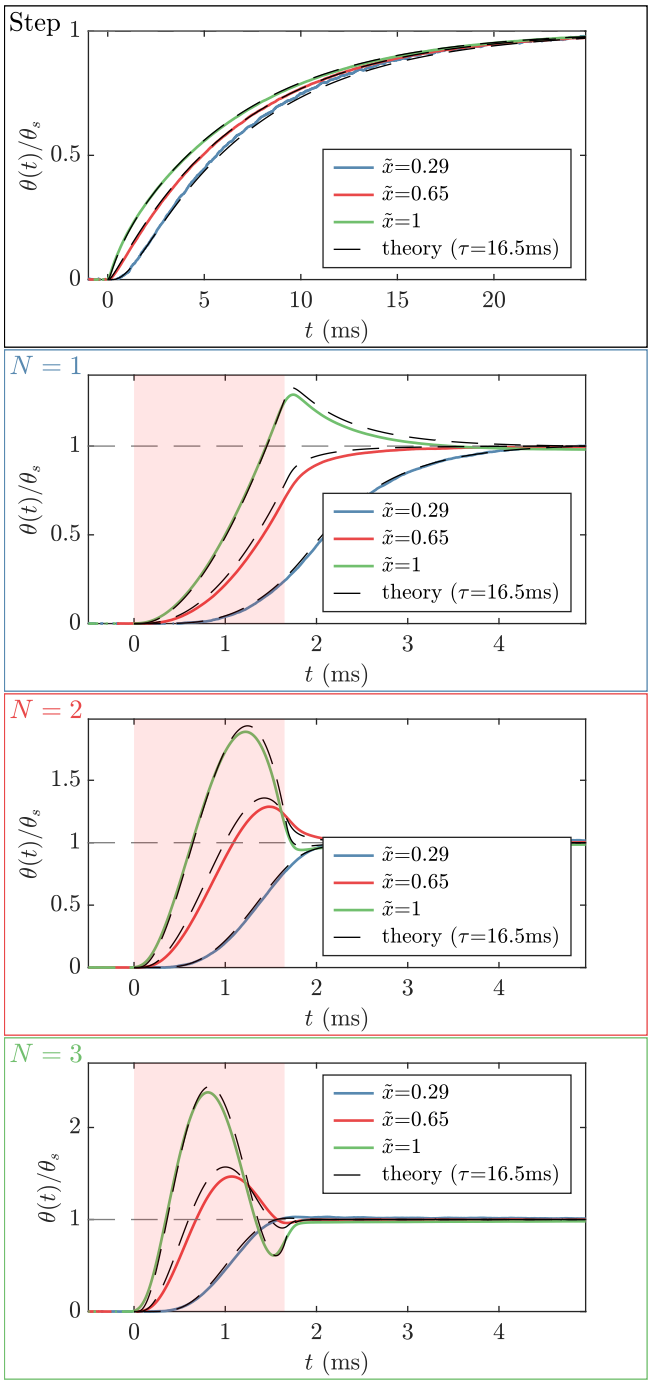


FIG. 8. Transient temperature profiles measured when applying a step function and the accelerating protocol ($N = 1$ up to $N = 3$) for a maximum temperature elevation $\theta_s^m = 1\,\mathrm{K}$. The small deviation from theory is attributed to the thermal conductivity dependence of silicon with temperature: as the initial profile corresponds to a maximum temperature rise of 50 K, λ is up to 16 % smaller near the cantilever's free end.

the freedom gained when the laser position $x_0(t)$ is no longer fixed but controlled in time: it would allow the required amount of heat to be deposited at each location of the cantilever, bypassing the slow diffusion process to reach the stationary state of the temperature field.

As a final consideration, let us rewind to our initial motivation: get closer or beat the time scales of the mechanical system. With an acceleration of a factor 30, the ratio of the mechanical and thermal time writes $T_0/t_f = 2\,\mu\mathrm{m}/H$. For our $H = 5\,\mu$m thick cantilever, we are thus able to stabilize the temperature field in only 2.5 oscillations, and we would reach half an oscillation with $H = 1\,\mu$m. As for the mechanical relaxation time τ_r which is Q/π times longer than the period T_0, with a quality factor of the order of $Q = 3000$ in our experiment in vacuum, we actually reach thermal steady state in $\tau_r/400$. Such an acceleration even allows stabilizing temperature faster than the "equilibration" of the first 12 mechanical resonant modes of the cantilever. Our strategy to accelerate the heat diffusion thus achieves its goal, and could be useful in numerous applications once we reach a meaningful temperature step amplitude.

The data that support the findings of this study are openly available in Zenodo [51].

ACKNOWLEDGMENTS

This work has been financially supported by the Agence Nationale de la Recherche through grant ANR-18-CE30-0013. C.A.P. acknowledges financial support from Grant No. PID2021-122588NB-I00 funded by MCIN/AEI/ 10.13039/501100011033/ and by "ERDF A way of making Europe", as well as funding from European Union for the support from Horizon Europe - Marie Sklodowska-Curie 2021 programme through the Posdoctoral Fellowship Ref. 101065902 (ORION). We thank Artyom Petrosyan, Salambô Dago, Ivan Palaia and Sergio Ciliberto for enlightening scientific and technical discussions.

APPENDIX

Appendix A: Coefficients γ_n of the polynomial function $F(t)$

Eq. 10 can be written as:

$$\sum_{m=1}^{N} A_{m,n}\gamma_m = 1, \text{ for } n = 1 \text{ to } N, \tag{A1}$$

$$\text{with } A_{m,n} = \int_0^1 s^{m-1} k_n^2 \tilde{t}_f e^{k_n^2 \tilde{t}_f (s-1)} ds. \tag{A2}$$

Using integrations by parts, we compute the coefficient $A_{m,n}$ analytically with the following recurrence relation:

$$A_{1,n} = 1 - e^{-k_n^2 \tilde{t}_f} \tag{A3}$$

$$A_{m+1,n} = 1 - \frac{m}{k_n^2 \tilde{t}_f} A_{m,n} \tag{A4}$$

The $N \times N$ square matrix A defined by its coefficients $A_{m,n}$ can then be inverted using a symbolic math solver, and the coefficients γ_m, solutions of $A[\gamma_m] = [1]$, computed analytically by $[\gamma_m] = A^{-1}[1]$. This approach avoids any rounding errors when computing the integrals in Eq. 10 or singularities when inverting the matrix A. Some examples of coefficients γ_m are given in Table I for $\tau/t_f = 10$ to 100 and $N = 1$ to 4, while Fig. 9 reports the maximum and minimum values of $F(t)$ for $\tau/t_f = 1$ to 1000 and $N = 1$ to 6.

As physically expected, shorter values for t_f or larger number N of modes canceled involve much greater costs. The maximum value of $F(t)$, always occurring at $t = 0$, behaves as $(\sqrt{N}t_f/\tau)^{-N}$. This scaling can be used to extrapolate the very large power requirements at strong accelerations and large mode numbers. From the theoretical point of view, no pathologies of any kind are found for the values obtained. However, from the practical point of view, very high intensities could lead to implementation problems for a standard experimental setup. Moreover, the assumption of constant thermal conductivity is jeopardized and non-linear effects beyond the simple heat equation considered herein should be taken into account.

		$N=1$	$N=2$	$N=3$	$N=4$
$\tau/t_f = 10$	γ_1	4.57	16.5	42	88.1
	γ_2		-22.9	-155	-585
	γ_3			122	1040
	γ_4				-548
$\tau/t_f = 30$	γ_1	12.7	113	641	2749
	γ_2		-198	-3204	-26156
	γ_3			2926	57017
	γ_4				-34647
$\tau/t_f = 100$	γ_1	41	1141	19361	238632
	γ_2		2191	-109748	-2662356
	γ_3			106680	6372575
	γ_4				-4126391

TABLE I. Coefficients γ_n of the polynomial function $F(t)$ found solving Eq. (10) that allow to cancel successively the four first thermal modes for a protocol duration t_f such that $\tau/t_f = 10$, $\tau/t_f = 30$ and $\tau/t_f = 100$.

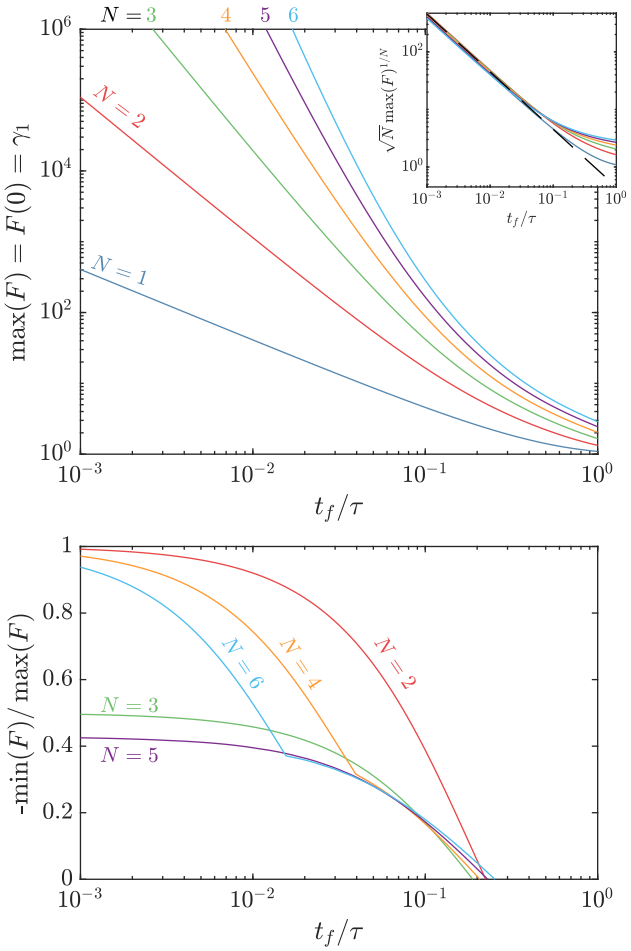


FIG. 9. (top) Maximum value of $F(t)$, corresponding to $F(0) = \gamma_1$, for $N = 1$ to 6 and $t_f/\tau = 10^{-3}$ to 1. Large N and short t_f lead to a huge range of power needed during the transient. A scaling $\max(F) \sim [0.45\tau/(t_f\sqrt{N})]^N$ is observed, as illustrated in the inset (dashed line is $0.45\tau/t_f$). (bottom) Minimum value of $F(t)$, normalized by its maximum value, for $N > 1$ (for $N = 1$, $F(t) > 0$ at all times - no cooling is necessary). The cooling power is always smaller in absolute value that the heating one.

Appendix B: Independence of the protocol on the laser location

In Fig. 10, we present a numerical check of the validity of our acceleration protocol for a different value of the laser location. More specifically, we take the same parameters as in the bottom panel of Fig. 4: $N = 4$, $t_f = 0.1\tau$, but $\tilde{x}_0 = 0.5$.

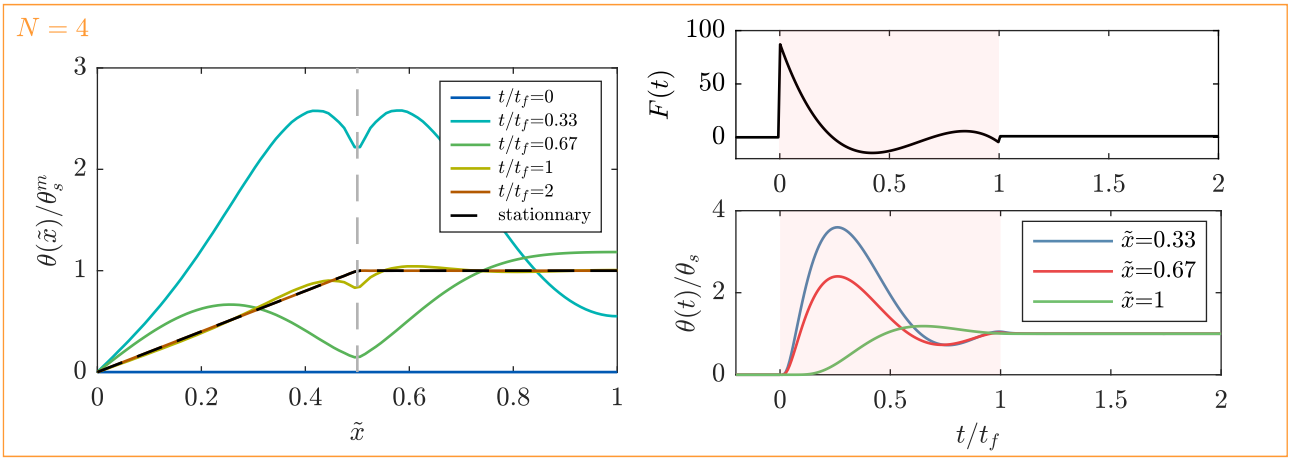


FIG. 10. Numerical simulation of the protocol for the same parameters as in the bottom panel of Fig. 4: $N = 4$, $t_f = 0.1\tau$, but a different value of the heating location, $\tilde{x}_0 = 0.5$.

Appendix C: Calibration of the sensitivity coefficient β

Since the cantilever thickness slightly varies along its length, the sensitivity coefficient β depends on the position x. To calibrate the function $\beta(x)$, we impose a uniform temperature profile (positioning the heating beam onto the chip) and we measure the induced change in reflectivity $\Delta R(x)$ at each location x. At the same time, we measure the shift of the mechanical resonance frequencies by analyzing the thermal noise driven fluctuations of position of the reflected probe beam. This frequency shift leads to a calibrated measurement of the imposed temperature change [16, 52]. The measured coefficients β to convert the reflectivity into temperature at all probed positions x are displayed in Fig. 11.

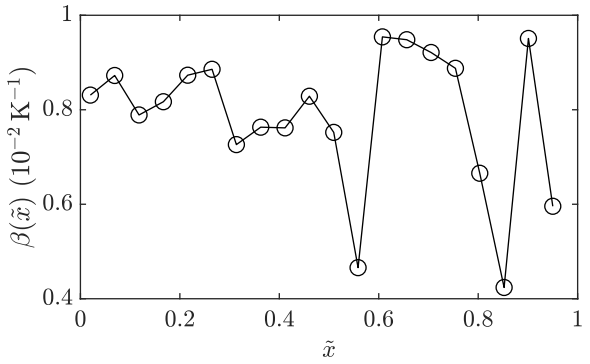


FIG. 11. Calibration of the sensitivity coefficient β. This quantity makes it possible to convert the variation of reflectivity into temperature change, $\theta(x) = \beta^{-1}(x)\Delta R(x)/R(x)$. The relatively large range of dispersion for the sensitivity β is mainly due to variations of the thickness along the cantilever length.

Appendix D: Transient temperature during the protocol

As illustrated in Figs. 4 and 7, the temperature can present overshoots and undershoots quite far from the target during (and after) the protocol. We plot in Fig. 12 the range of temperature explored according to the numerical resolution of the heat equation for the drivings defined in Appendix A. Transient temperatures can be orders of magnitude larger than the target step, limiting the applicability of very fast acceleration to small θ_s.

As a further insight in the dynamics of the temperature and the acceleration provided by our protocols, we report in Fig. 13 the time to reach the target with a 2% tolerance. This time depends on the choice of t_f and N obviously, but also on the relaxation of remaining modes

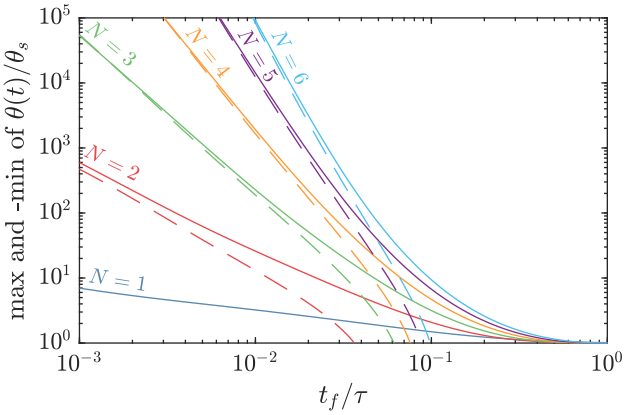


FIG. 12. Maximum (plain line) and opposite of the minimum (dashed line) values of $\theta(t)$ for $N = 1$ to 6, $t_f/\tau = 10^{-3}$ to 1, and $\tilde{x}_0 = 0.95$. Large N and short t_f lead to a huge transient temperature, limiting the magnitude of achievable temperature step θ_s. No negative values of $\theta(t)$ are observed for $N = 1$.

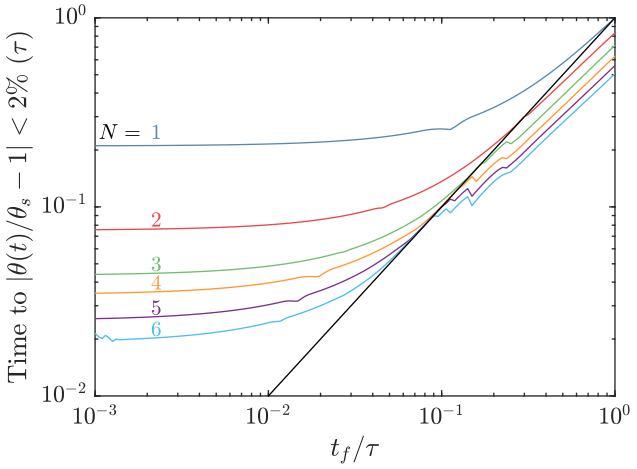


FIG. 13. Time (in units of τ) to reach the target with a 2% tolerance for $N = 1$ to 6, $t_f/\tau = 10^{-3}$ to 1, and $\tilde{x}_0 = 0.95$. This time is defined as the latest instant when $|\theta(t,x)/\theta_s(x) - 1| > 2\%$, for $x = 0.33$, 0.67 and x_0. $\theta(t,x)$ is computed from numerical resolution of the heat equation for the drivings defined in Appendix A. Achieving this goal requires 1.8τ with a power step protocol, and 0.4τ with a perfect feedback loop (temperature step protocol). The black line is the duration of the protocol t_f/τ: curves below it reach the target actually faster than the protocol itself.

after t_f. For very large acceleration ($t_f < \tau/100$), the amplitude of the remaining temperature field at t_f is significant and though decaying very fast, further delays the effective reach of the vicinity of the target. Effective accelerations over 100 are thus out of reach in practice.

Appendix E: Response to a temperature step (perfect feedback loop)

We provide here the solution for the heat equation (1) without a source term:

$$\partial_t \theta = D\partial_x^2 \theta, \tag{E1}$$

with $D = \lambda/(\rho c_p)$ and the following boundary conditions:

$$\theta(0,t) = 0, \quad \theta(x_0,t) = \theta_s^m, \quad \partial_x \theta(x,t)|_{x=L} = 0, \tag{E2}$$

with $0 < x_0 < L$, and initial condition:

$$\theta(x,0) = 0. \tag{E3}$$

Note that, since there is an extra "boundary" condition at $x = x_0$, i.e. within the interval $0 \le x \le L$, the equation should be solved separately for the two intervals $0 \le x < x_0$ and $x_0 < x \le L$. The stationary solution is

$$\frac{\theta_s(x,t)}{\theta_s^m} = \begin{cases} \frac{x}{x_0} & 0 \le x \le x_0, \\ 1 & x_0 \le x \le L \end{cases} \tag{E4}$$

After expanding $\Delta\theta(x,t) = \theta(x,t) - \theta_s(x)$ in the corresponding eigenbasis, one gets

$$\frac{\theta(x,t)}{\theta_s^m} = \begin{cases} \dfrac{x}{x_0} + \dfrac{2}{\pi}\displaystyle\sum_{n=1}^{\infty} \dfrac{(-1)^n}{n} \sin\left(n\pi \dfrac{x}{x_0}\right) \exp\left(-\dfrac{n^2\pi^2 D}{x_0^2} t\right) & 0 \le x \le x_0, \\ 1 - \dfrac{4}{\pi}\displaystyle\sum_{n=1}^{\infty} \dfrac{1}{2n-1} \sin\left[\left(n - \dfrac{1}{2}\right)\pi \dfrac{x - x_0}{L - x_0}\right] \exp\left[-\dfrac{(2n-1)^2\pi D}{4(L-x_0)^2} t\right] & x_0 \le x \le L \end{cases} \tag{E5}$$

Characteristic relaxation times to the left and to the right of the point x_0 are proportional to $\tau_{\text{left}} = x_0^2/D$ and $\tau_{\text{right}} = (L - x_0)^2/D$ respectively. With respect to the power step solution, assuming $x_0 \sim L$, the slowest time constant in the exponentially decaying functions is four time smaller. This acceleration stems from the change of modes from $k_n = (n - 1/2)\pi$ to $k_n = n\pi$, due to the change of the relevant boundary condition from Neumann to Dirichlet.

Rather than considering Eq. (E1) separately in the intervals $0 \le x < x_0$ and $x_0 < x \le L$, we could have instead considered Eq. (1) complemented with Eq. (2), i.e. with a localized $\delta(x - x_0)$ forcing term proportional to $P(t)$. Thus, the perfect feedback loop introduced in this appendix can be experimentally implemented with a feedforward protocol with the laser power

$$P(t) = \frac{\lambda S \theta_s^m}{a}\left[\frac{\vartheta_3(e^{-\frac{D\pi^2 t}{x_0^2}})}{x_0} + \frac{\vartheta_2(e^{-\frac{D\pi^2 t}{(L-x_0)^2}})}{L - x_0}\right]. \tag{E6}$$

This latter relation is obtained from direct integration of the heat equation (1) over an infinitesimal interval around x_0, substituting for $\theta(x,t)$ the solution (E5). Above, $\vartheta_a(q)$, with $a \in \{2,3\}$ stands for the elliptic theta function $\Theta_a(u,q)$ evaluated in $u = 0$: $\vartheta_a(q) = \Theta_a(0,q)$, with

$$\Theta_2(u,q) = 2q^{1/4}\sum_{n=0}^{\infty} q^{n(n+1)} \cos[(2n+1)u], \tag{E7}$$

$$\Theta_3(u,q) = 1 + 2\sum_{n=1}^{\infty} q^{n^2} \cos(2nu). \tag{E8}$$

[1] W. M. Haynes, ed., *CRC Handbook of Chemistry and Physics*, 95th ed. (CRC Press, Boca Raton, 2014).

[2] G. Binnig, C. F. Quate, and C. Gerber, Atomic force microscope, Phys. Rev. Lett. **56**, 930 (1986).

[3] G. Meyer and A. Nabil M., Novel optical approach to atomic force microscopy, Appl. Phys. Lett. **53**, 1045 (1988).

[4] O. Marti, A. Ruf, M. Hipp, H. Bielefeldt, J. Colchero, and J. Mlynek, Mechanical and thermal effects of laser irradiation on force microscope cantilevers, Ultramicroscopy **42–44**, 345 (1992).

[5] M. Allegrini, C. Ascoli, P. Baschieri, F. Dinelli, C. Frediani, A. Lio, and T. Mariani, Laser thermal effects on atomic force microscope cantilevers, Ultramicroscopy **42–44**, 371 (1992).

[6] B. McCarthy, Y. Zhao, R. Grover, and D. Sarid, Enhanced raman scattering for temperature measurement of a laser-heated atomic force microscope tip, Appl. Phys. Lett. **86**, 111914 (2005).

[7] D. Ramos, J. Tamayo, J. Mertens, and M. Calleja, Photothermal excitation of microcantilevers in liquids, J. Appl. Phys. **99**, 124904 (2006).

[8] J. Lee, T. L. Wright, M. R. Abel, E. O. Sunden, A. Marchenkov, S. Graham, and W. P. King, Thermal conduction from microcantilever heaters in partial vacuum, J. Appl. Phys. **101**, 014906 (2007).

[9] A. A. Milner, K. Zhang, V. Garmider, and Y. Prior, Heating of an Atomic Force Microscope tip by femtosecond laser pulses, Appl. Phys. A **99**, 1 (2010).

[10] D. Kiracofe, K. Kobayashi, A. Labuda, A. Raman, and H. Yamada, High efficiency laser photothermal excitation of microcantilever vibrations in air and liquids, Rev. Sci. Instrum. **82**, 013702 (2011).

[11] B. A. Bircher, L. Duempelmann, H. P. Lang, C. Gerber, and T. Braun, Photothermal excitation of microcantilevers in liquid: effect of the excitation laser position on temperature and vibrational amplitude, Micro & Nano Letters **8**, 770 (2013).

[12] R. García and R. Pérez, Dynamic atomic force microscopy methods, Surf. Sci. Rep. **47**, 197 (2002).

[13] Silicon is the most common material for AFM cantilevers.

[14] X. Chen and X. Wang, Microscale spatially resolved thermal response of si nanotip to laser irradiation, J. Phys. Chem. C **115**, 22207 (2011).

[15] S. Gomès, A. Assy, and P.-O. Chapuis, Scanning thermal microscopy: A review, Phys. Status Solidi (A) **212**, 477 (2015).

[16] F. Aguilar Sandoval, M. Geitner, E. Bertin, and L. Bellon, Resonance frequency shift of strongly heated microcantilevers, J. Appl. Phys. **117**, 234503 (2015).

[17] K. Sekimoto, *Stochastic Energetics*, Lecture Notes in Physics, Vol. 799 (Springer, 2010).

[18] M. Rademacher, M. Konopik, M. Debiossac, D. Grass, E. Lutz, and N. Kiesel, Nonequilibrium control of thermal and mechanical changes in a levitated system, Phys. Rev. Lett. **128**, 070601 (2022).

[19] T. Schmiedl and U. Seifert, Efficiency at maximum power: An analytically solvable model for stochastic heat engines, EPL (Europhysics Letters) **81**, 20003 (2007).

[20] S. Toyabe, T. Sagawa, M. Ueda, M. Muneyuki, and M. Sano, Experimental demonstration of information-to-energy conversion and validation of the generalized Jarzynski equality, Nat. Phys. **6**, 988 (2010).

[21] M. Esposito, R. Kawai, K. Lindenberg, and C. Van den Broeck, Efficiency at maximum power of low-dissipation carnot engines, Phys. Rev. Lett. **105**, 150603 (2010).

[22] V. Blickle and C. Bechinger, Realization of a micrometre-sized stochastic heat engine, Nat. Phys. **8**, 143 (2012).

[23] M. Esposito, N. Kumar, K. Lindenberg, and C. Van den Broeck, Stochastically driven single-level quantum dot: A nanoscale finite-time thermodynamic machine and its various operational modes, Phys. Rev. E **85**, 031117 (2012).

[24] V. Holubec, An exactly solvable model of a stochastic heat engine: optimization of power, power fluctuations and efficiency, J. Stat. Mech. **2014**, P05022 (2014).

[25] I. A. Martínez, E. Roldán, L. Dinis, D. Petrov, and R. A. Rica, Adiabatic processes realized with a trapped brownian particle, Phys. Rev. Lett. **114**, 120601 (2015).

[26] I. A. Martínez, É. Roldán, L. Dinis, D. Petrov, J. M. R. Parrondo, and R. A. Rica, Brownian carnot engine, Nat. Phys. **12**, 67 (2016).

[27] C. A. Plata, D. Guéry-Odelin, E. Trizac, and A. Prados, Building an irreversible carnot-like heat engine with an overdamped harmonic oscillator, J. Stat. Mech. **2020**, 093207 (2020).

[28] D. Guéry-Odelin, C. Jarzynski, C. A. Plata, A. Prados, and E. Trizac, Driving rapidly while remaining in control: classical shortcuts from hamiltonian to stochastic dynamics, Rep. Prog. Phys. **86**, 035902 (2023).

[29] S. Dago, J. Pereda, N. Barros, S. Ciliberto, and L. Bellon, Information and thermodynamics: Fast and precise approach to landauer's bound in an underdamped micromechanical oscillator, Phys. Rev. Lett. **126**, 170601 (2021).

[30] E. Aurell, K. Gawedzki, C. Mejía-Monasterio, R. Mohayaee, and P. Muratore-Ginanneschi, Refined second law of thermodynamics for fast random processes, J. Stat. Phys. **147**, 487 (2012).

[31] U. Seifert, Stochastic thermodynamics, fluctuation theorems and molecular machines, Rep. Prog. Phys. **75**, 126001 (2012).

[32] C. Jarzynski, Equalities and inequalities: Irreversibility and the second law of thermodynamics at the nanoscale, Ann. Rev. Cond. Matt. Phys. **2**, 329 (2011).

[33] S. Dago and L. Bellon, Dynamics of information erasure and extension of landauer's bound to fast processes, Phys. Rev. Lett. **128**, 070604 (2022).

[34] S. Dago, J. Pereda, S. Ciliberto, and L. Bellon, Virtual double-well potential for an underdamped oscillator created by a feedback loop, J. Stat. Mech. **2022**, 053209 (2022).

[35] In this expression, adiabatic is to be understood in the sense of a slow transformation.

[36] X. Chen, A. Ruschhaupt, S. Schmidt, A. del Campo, D. Guéry-Odelin, and J. G. Muga, Fast Optimal Frictionless Atom Cooling in Harmonic Traps: Shortcut to Adiabaticity, Phys. Rev. Lett. **104**, 063002 (2010).

[37] D. Guéry-Odelin, A. Ruschhaupt, A. Kiely, E. Torrontegui, S. Martínez-Garaot, and J. Muga, Shortcuts to adiabaticity: Concepts, methods, and applications, Rev. Mod. Phys. **91**, 045001 (2019).

[38] D. Guéry-Odelin, J. G. Muga, M. J. Ruiz-Montero, and E. Trizac, Nonequilibrium Solutions of the Boltzmann Equation under the Action of an External Force, Phys. Rev. Lett. **112**, 180602 (2014).

[39] I. A. Martínez, A. Petrosyan, D. Guéry-Odelin, E. Trizac, and S. Ciliberto, Engineered swift equilibration of a Brownian particle, Nat. Phys. **12**, 843 (2016).

[40] A. Patra and C. Jarzynski, Shortcuts to adiabaticity using flow fields, New J. Phys. **19**, 125009 (2017).

[41] G. Li, H. T. Quan, and Z. C. Tu, Shortcuts to isothermality and nonequilibrium work relations, Phys. Rev. E **96**, 012144 (2017).

[42] S. González-Resines, D. Guéry-Odelin, A. Tobalina, I. Lizuain, E. Torrontegui, and J. G. Muga, Invariant-based inverse engineering of crane control parameters, Phys. Rev. Appl. **8**, 054008 (2017).

[43] I. Palaia, *Charged systems in, out of, and driven to equilibrium: from nanocapacitors to cement*, Ph.D. thesis, Paris-Saclay University (2019).

[44] D. Xiong, F. Thiel, and E. Barkai, Using hilbert transform and classical chains to simulate quantum walks, Phys. Rev. E **96**, 022114 (2017).

[45] A. Krivtsov, The ballistic heat equation for a one-dimensional harmonic crystal, in *Dynamical Processes in Generalized Continua and Structures*, edited by H. Altenbach, A. Belyaev, V. A. Eremeyev, A. Krivtsov, and A. V. Porubov (Springer International Publishing, Cham, 2019) pp. 345–358.

[46] A. Gal and O. Raz, Precooling strategy allows exponentially faster heating, Phys. Rev. Lett. **124**, 060602 (2020).

[47] B. Pottier and L. Bellon, Thermo-optical bistability in silicon micro-cantilevers, SciPost Phys. **10**, 120 (2021).

[48] Movies supplied as ancillary files: `tf=0.1tau-N=X.mov`, with `X=1` to `4`, compare the time evolution of the temperature profile for a power step, a temperature step (perfect feedback loop), and our acceleration protocols for $N = 1$ to 4.

[49] A. Masolin, P.-O. Bouchard, R. Martini, and M. Bernacki, Thermo-mechanical and fracture properties in single-crystal silicon, J. Mater. Sci. **48**, 979 (2013).

[50] X. Wang and B. Huang, Computational Study of In-Plane Phonon Transport in Si Thin Films, Sci. Rep. **4**, 6399 (2014).

[51] B. Pottier, C. A. Plata, E. Trizac, D. Guéry-Odelin, and L. Bellon, Dataset for *Phys. Rev. Applied* **19**, 034072 (2023) - Accelerating the heat diffusion: Fast thermal relaxation of a microcantilever, Zenodo, doi:10.5281/zenodo.7669038 (2023).

[52] B. Pottier, F. Aguilar Sandoval, M. Geitner, F. Esteban Melo, and L. Bellon, Silicon cantilevers locally heated from 300k up to the melting point: Temperature profile measurement from their resonances frequency shift, J. Appl. Phys. **129**, 184503 (2021).